Proceedings of the 28th IEEE
EMBS Annual International Conference
New York City, USA, Aug 30-Sept 3, 2006

Robust Contact Detection in Micromanipulation Using Computer Vision Microscopy

W. H. Wang, X. Y. Liu, *Student Member, IEEE*, and Y. Sun, *Member, IEEE*

***Abstract*—This paper presents a computer vision algorithm for visually detecting the contact between an end-effector and a target surface under an optical microscope. Without using additional sensors (e.g., proximity or force/touch sensors), this algorithm provides robustness and a sub-micrometer detection resolution. Fundamentally, after the establishment of a contact in the world frame, further vertical motion induces horizontal motion in the image plane. An analysis is presented to elaborate this fundamental mechanism. Experimental results demonstrate that this computer-vision-based method is capable of achieving contact detection between a micropipette and a glass slide surface with a resolution of 0.2μm. Furthermore, 1300 experimental trials reveal that the presented algorithm is robust to variations in illumination intensity, microscopy magnification, and microrobot motion speed.**

I. Introduction

AUTONOMOUS manipulation of micrometer sized objects is essential in both biological/engineering research and for the commercial success of many microscaled technologies. In microrobotic manipulation, an end-effector, such as a MEMS-based microgripper or a glass micropipette controlled by a microrobot is used to interact with micro objects.

The schematic in Fig. 1 shows a biological cell held in a micropatterned cavity for microrobotic cell injection or single cell biomechanics studies [1]. To position the micropipette in the desired plane (e.g., the bisecting plane in Fig. 1), the relative vertical positions of the micropipette tip and the device surface must be precisely determined. Detection of the contact between the micropipette tip and the surface is the focus of this paper.

Existing methods employ proximity sensors [2], [3], piezoresistive sensors [4], or piezoelectric touch sensors [5] to determine the relative coordinates between the end-effector and the target surface. The integration of sensors with end-effectors is often difficult and complicates system setup. As contact-type sensors [3], [4], [5] at the microNewton levels are fragile and prone to damage, extra care must be taken in sensor overloading protection. Furthermore, reported contact detection resolutions using additional sensors are limited to a few microns, calling for methods capable of providing a better detection resolution without using additional sensors.

As microrobotic cell manipulation and the assembly of microsystems are universally conducted under an optical microscope that provides high-resolution, low depth-of-field visual feedback, it is highly desirable to use microscopy visual feedback for contact detection without using additional sensors. Assuming that the micropipette tip and the target (i.e., glass slide surface) share the same focal plane, autofocusing algorithms can be used to independently servo the micropipette tip and the glass slide surface in order to bring them to a co-plane.

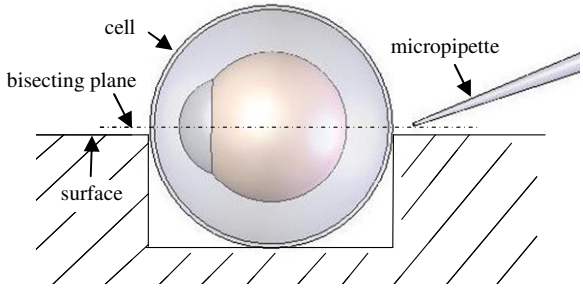

Fig. 1. Relative vertical positions of the micropipette tip and the device surface for microrobotic cell manipulation.

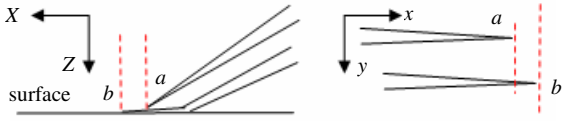

Fig. 2. Side view of tip and surface (left). Top view in image plane (right).

However, autofocusing algorithms are sensitive to illumination conditions (angle of incidence and intensity) and feature selections for calculating focus measures, making autofocusing-based contact detection lack robustness. More importantly, the depth of field of an optical microscope is often on the order of a few microns, which makes images of two objects with different world coordinates reveal sharpness over a distance of micrometers. Thus, focus-measure-based methods are not capable of precisely bringing the micropipette tip and the glass slide surface to a co-plane.

This paper reports a computer vision algorithm that addresses the detection of contact between an end-effector and a target surface. The fundamental rationale is based on the experimental observation that horizontal motion in the image plane occurs upon the establishment of a contact. As shown in Fig. 2, upon contact, further motion along the vertical direction (Z) is translated to horizontal motion along the X direction. This observation is not limited to contact between a micropipette tip and a glass slide surface although such a setup is used as an example to illustrate the algorithm.

II. Contact Detection Analysis

Fig. 3 shows a schematic consisting of an image plane,

The authors are with the Advanced Micro and Nanosystems Laboratory at the University of Toronto. 5 King's College Road, Toronto, Ontario, Canada, M5S 3G8 (phone: 1-416-946-0549; e-mail: sun@mie.utoronto.ca)

microscope objective, and the object (micropipette tip). When the tip is controlled to move downwards at a constant speed, corresponding positions of the tip are labeled as Position 1, 2, and 3 in both the world frame (*X*-*Y*-*Z*) and the image plane (*x*-*y*). Position 3 corresponds to exact contact. Taking '0' as the origin of the image plane, it is evident that the *x* coordinate keeps decreasing prior to contact.

The displacement along the *Z* direction in the world frame between two successive positions is denoted by Δh. The distance between the tip at Position 1 and the objective is denoted by *u*. The horizontal distance between the tip and the optical axis is denoted by X_0. The distance between the image plane and the objective is denoted by *v*. When $\Delta h \ll u$, decrements of the *x* coordinates in the image plane are

$$\Delta x_{21} = \frac{v \cdot \Delta h \cdot X_0}{u \cdot (u + \Delta h)} \approx \frac{v}{u^2} \cdot X_0 \cdot \Delta h \tag{1}$$

$$\Delta x_{32} = \frac{v \cdot \Delta h \cdot X_0}{(u + 2 \cdot \Delta h) \cdot (u + \Delta h)} \approx \frac{v}{u^2} \cdot X_0 \cdot \Delta h \tag{2}$$

Comparing (1) and (2), the two decrements are approximately equal, which implies that prior to contact, the *x* coordinates of the tip decrease in proportion to the downward displacements along *Z* in the world frame.

Upon contact at Position 3, further downward motion will make the tip slide along the surface, for example, to Position 4 and 5 (Fig. 3(b)). As '0' is taken as the origin of the image plane, it is evident now that the *x* coordinate starts to consistently increase after contact. The *x*-coordinate increments in the image plane are

$$\Delta x_{43} = \frac{v}{(u + 2 \cdot \Delta h)} \cdot X_{43} \approx \frac{v}{u} \cdot X_{43} \tag{3}$$

$$\Delta x_{54} = \frac{v}{(u + 2 \cdot \Delta h)} \cdot X_{54} \approx \frac{v}{u} \cdot X_{54} \tag{4}$$

Assume the micropipette tip establishes the initial contact at *AB* and deforms into a contour of *A'B'* (Fig. 3(c)). *BB'* is the distance that the tip slides along the *X* direction. X_{43} and X_{54} can be expressed as

$$X_{43} = X_{54} = \Delta h \cdot ctg((\pi - \theta)/2) = \Delta h \cdot \tan(\theta/2) \tag{5}$$

Substituting (5) into (3) and (4) yields

$$\Delta x_{43} = v/u \cdot \Delta h \cdot \tan(\theta/2) \tag{6}$$

$$\Delta x_{54} = v/u \cdot \Delta h \cdot \tan(\theta/2) \tag{7}$$

Comparing (6) and (7), the two increments are equal, implying that after contact, the *x* coordinates of the tip increase in proportion to the downward displacements along *Z* in the world frame.

In summary, the analysis demonstrates that it is when the micropipette tip reaches the minimal *x*-coordinate value in the image plane that initial contact occurs between the tip and the target surface.

III. Experimental Setup

The system, shown in Fig. 4 consists of a stage holding a glass slide, an optical microscope (Olympus SZX12) with a CMOS digital camera (Basler A601f), and a three-degrees-of-freedom microrobot with a travel of 25mm and a 0.04μm positioning resolution along each axis (MP-285, SUTTER). The microrobot is controlled via a motion control board (NI PCI-6259), carrying a glass micropipette (TW120F-4). The system setup is mounted on a vibration isolation table.

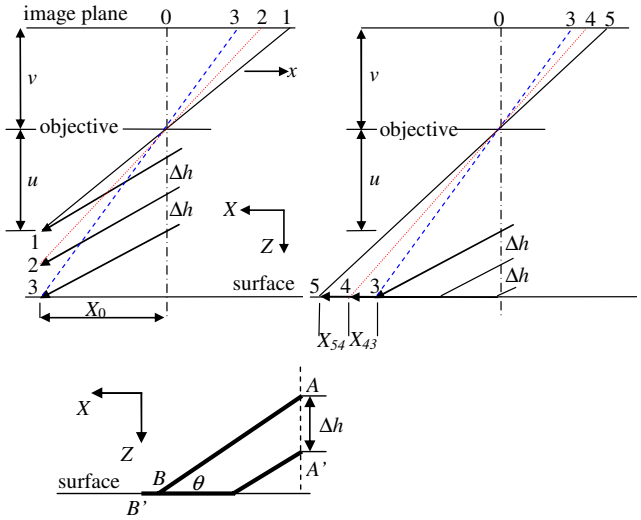

Fig. 3. An optical model for contact detection analysis. Top left: prior to contact. Top right: after contact. Bottom: tip deformation after contact.

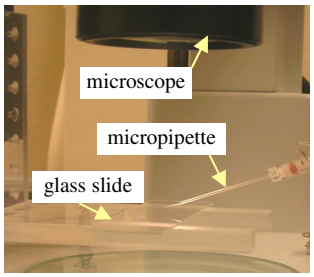

Fig. 4. Experimental setup.

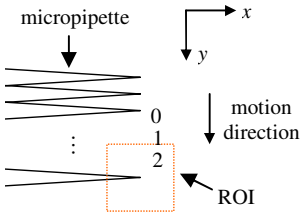

Fig. 5. Pipette moving in image plane.

IV. Tip Area Identification

In order to identify the region of interest (ROI) surrounding the micropipette for further contact detection, an identification algorithm is developed. The micropipette is moved by the microrobot horizontally (*Y*) at a constant speed without any *Z* movement. In the image plane, the micropipette moves along the *y* direction, as shown in Fig. 5. Full-frame images (640×480) are processed in real time (30Hz) for locating the ROI that contains the pipette tip. In this procedure, the pipette tip is not necessarily required to be in-focus. Instead, as long as the contour of the tip is visible, the ROI can be robustly identified.

Image frames are denoted by $I(x, y, t)$, where $t = 0, 1, 2\ldots$ Each image frame is first convolved with a low-pass Gaussian filter for noise suppression. The resulting image is denoted by $F(x, y, t)$ (Fig. 6(a)(b)). For two successive frames in an image sequence, their gray-level differences with respect to the very first frame (t=0) are

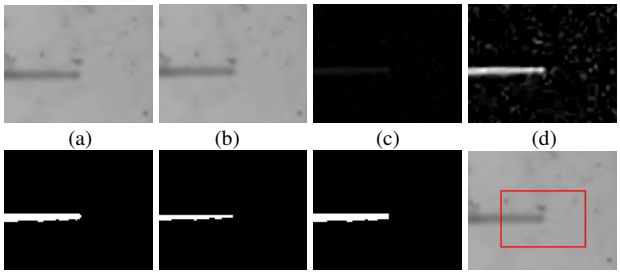

Fig. 6. Sequence for locating the ROI. **(a)** Frame 0 (unfocused pipette tip). **(b)** Frame 4. **(c)** Differentiation image between (b) and (a). **(d)** Image after contrast stretching of (c). **(e)** Thresholded image of (d). **(f)** Erosion image of (e). **(g)** Dilation image of (f). **(h)** ROI found at frame 4.

$$D(t+1) = F(x, y, t+1) - F(x, y, 0) \tag{8}$$

$$D(t) = F(x, y, t) - F(x, y, 0) \tag{9}$$

For each differentiation image $D(t)$ and $D(t+1)$ (Fig. 6(c)), the following processing steps are conducted. **Step A.** *Contrast stretching* [6] is used to increase the dynamic range of the gray levels in the differentiation image (Fig. 6(d)). **Step B.** *Thresholding*: adaptive optimal threshold determination is conducted based on the Otsu method [7] (Fig. 6(e)). **Step C.** *Morphology*: an erosion operation [6] is used to remove small areas regarded as noises that can produce many artificial separate objects (Fig. 6(f)). A dilation operation [6] is then used to connect broken segments that originally are of one object (Fig. 6(g)). **Step D.** *Tip recognition*: As the pipette keeps moving along Y, the number of objects detected in the image decreases dramatically. When the number of objects decreases by 90% in two successive frames, the object with the maximum area is recognized as the micropipette tip. The tip is located on the rightmost end of the micropipette in the experiments. A ROI of 100×80 (Fig. 6(h)) around the tip is then chosen for subsequent contact detection. In the case given in Fig. 6, the ROI was found at frame 4 (i.e., t=4).

After the determination of ROI, the micropipette stops moving along the Y direction. It is then controlled to move in downward direction (Z) at a *constant* speed to achieve contact with the surface. In the following contact detection process described in Section V, image processing is only conducted inside the ROI to alleviate computation complexity and allow real-time performance (30Hz).

V. Contact Detection

As shown in Fig. 2, upon contact, the tip is at location a. After the establishment of contact, the tip slides horizontally on the surface and deviates from location a to b. Contact detection leverages such changes in the x coordinate. As analyzed in Section II, physical contact occurs when the tip reaches its minimal x-coordinate value in the image. To locate the minimal value, the pipette moves downwards at a *constant* speed until its x-coordinate surpasses the minimal value by a few pixels (e.g., 6 pixels). More pixels represent larger micropipette tip deformations that can lead to micropipette breakage. During this process, the precise Z positions of the microrobot corresponding to each frame of image are recorded. Thus, the microrobot can precisely bring the micropipette tip back to the exact contact position after the completion of contact detection.

TABLE I Processing Steps for Contact Detection

Step #	Processing
1	Gaussian low-pass filtering
2	Thresholding using the Otsu method [7]
3	Morphology (erosion and dilation)
4	Tip's x coordinate in image update
5	If current x coordinate exceeds the minimal value by 6 pixels, moving the micropipette back to the Z position of the contact point corresponding to the minimal value. Otherwise, update the minimal x value and go back to Step #1

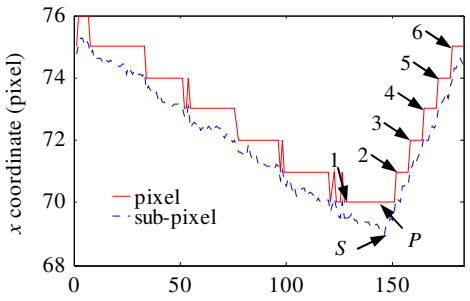

Fig. 7. Tip x-coordinate changes vs. frame index when moving downwards along Z in world frame. (speed: 14μm/s, magnification: 9×)

TABLE II Tip Displacement for One Pixel Increase in Fig. 7

Adjacent points of one-pixel away	2-3	3-4	4-5	5-6
Physical displacement along Z (μm)	2.4	2.8	2.4	2.8

The process flow for contact detection is described in Table I. Note that ROIs of images $I(x,y,t)$ are processed rather than the differentiation images $D(x,y,t)$. In Step 4, the micropipette tip is selected by searching for the most significant object in the ROI. Inside the ROI, tasks include: 1) to determine the tip's x-coordinate value using either a pixel-accuracy method or a sub-pixel-accuracy method that will be discussed in the following two sub-sections; 2) to compare the current x-coordinate value with the current minimal value and update this minimal value, if needed.

A. Locating the Tip with Pixel Accuracy

An experimental curve of changes in the x coordinate vs. frame index is shown in Fig. 7. Point 1 corresponds to the first frame in the valley. Point 2 is one pixel above the valley. Similarly, Point 6 is five pixels above the valley. The valley lasts a number of frames between Point 1 and Point 2. Within this valley band lies the exact contact point that can be determined by interpreting (6) and (7).

Examining (6) and (7) reveals that after contact, each increment of one pixel in the x coordinate of the image plane corresponds to an equal displacement along the Z direction in the world frame. Corresponding to Fig. 7, physical displacements along the Z direction and their corresponding frame indices are given in Table II.

Thus, the frame index for the contact point (P in Fig. 7), f_P can be obtained as $f_2 - N$, where f_2 is the frame index for Point 2, and N is the number of frames between Point 2 and Point 3. However, as the number of frames between Point 2 and Point 3 and the one between Point 3 and Point 4 are not strictly equal, numbers of frames per pixel step are averaged to reduce the error of f_P

$$f_P = f_2 - (f_6 - f_2)/4 \tag{10}$$

where f_6 is the frame index for Point 6.

B. Locating the Tip with Sub-Pixel Accuracy

Using (10) to determine the contact point involves several image frames and the accuracy is limited due to the fact that numbers of frames between Point 2 and 3… and between Point 5 and 6 are slightly different. In order to further improve the detection accuracy, an edge detection algorithm [8] is employed to locate the micropipette tip with sub-pixel accuracy in the image plane. Thus, the contact point (S in Fig. 7) is determined as a valley point rather than through a search in a valley band.

C. Performance Evaluation

To evaluate the performance of the image-based contact detection algorithms, effects of variations in illumination intensity, microrobot motion speed in lowering the micropipette, and magnifications of the microscope on detection accuracy were experimentally investigated. Experiments were repeated 50 times for studying each effect. Totally, 1300 experimental trials were conducted.

Experimental results demonstrate that the sub-pixel-accuracy method outperforms the pixel-accuracy method. Both algorithms are not significantly affected by illumination intensity variations. A very high motion speed produces a higher standard deviation. Finally, a higher magnification provides more accurate contact detection results.

The proposed image-processing-based contact detection method is robust. In all the 1300 experimental trials, contact detection was achieved without the occurrence of micropipette tip breakage using both the pixel-accuracy method and sub-pixel-accuracy method. For the majority of the trials, the standard deviation ranged from 0.87μm to 2.0μm. When the motion speed was high (380μm/s), the largest standard deviation occurred (12.4μm for the pixel-accuracy method; 9.8μm for the sub-pixel-accuracy method). This high speed produced a significant vertical displacement (12.7μm) along Z in the world frame between two successive image frames, causing a large contact detection deviation.

D. Validation

In the validation experiments, the micropipette was controlled by the microrobot to move downwards at a speed of 14μm/s. A magnification of 3.2× was used. Using the image-based contact detection method, 100 iterations of experiments were conducted (50 times using the pixel-accuracy methods; 50 times using the sub-pixel-accuracy method) in each trial group (3 trial groups total). The mean values of the located contact points are given in Table III.

TABLE III Z READINGS FOR CONTACT POINTS (μm)

Trial group #	Balance-measured position	Pixel-accuracy method	Sub-pixel method
1	2961.0	2958.2	2961.4
2	3031.0	3029.4	3031.2
3	3030.0	3029.4	3031.2

In order to verify the accuracies of the image-processing located contact points, the glass slide was then placed on an analytical balance (XP205, Mettler Toledo) with a 0.01mg (0.1μN) resolution. In Table III, the 'real' contact positions were determined by detecting a 0.01mg contact force change of the balance. A resolution as good as 0.2μm was achieved.

VI. CONCLUSION

This paper presented a computer vision algorithm for visually detecting the contact between an end-effector and a target surface under an optical microscope without using additional proximity or force/touch sensors. The rationale behind the algorithm is based on the fact that after the establishment of a contact, further vertical motion in the world frame induces horizontal motion in the image plane. Without requiring the object be in focus, the algorithm starts with the determination of a region of interest, and then further detects the contact using either a pixel-accuracy or a sub-pixel-accuracy method. Experiments demonstrated that the computer-vision-based method is capable of achieving contact detection between a micropipette tip and a glass slide surface with a resolution of 0.2μm. Furthermore, 1300 experimental trials revealed that the algorithm is robust to variations in illumination intensity, microscopy magnification, and microrobot motion speed.

REFERENCES

[1] Y. Sun, and B. J. Nelson, "Biological cell injection using an autonomous microrobotic system," *International Journal of Robotics Research*, vol. 21, no. 10-11, pp. 861-868, 2002.

[2] G. Trummer, C. Kurzals, R. Gehring, and D. Leistner, "Next-generation proximity and position sensors," *Sensors*, vol. 21, no. 3, pp. 14-21, 2004.

[3] Y. F. Li, "A sensor-based robot transition control strategy," *Int. J. of Robotics Research*, vol. 15, no. 2, pp. 128-136, 1996.

[4] M. Sitti, and H. Hashimoto, "Two-dimensional fine particle positioning under optical microscope using a piezoresistive cantilever as a manipulator," *J. Micromechatron*., vol. 1, no. 1, pp. 25-48, 2000.

[5] F. Arai, K. Motoo, P. G. R. Kwon, T. Fukuda, A. Ichikawa, and T. Katsuragi, "Novel touch sensor with piezoelectric thin film for microbial separation," in *IEEE Int. Conf. on Robotics and Automation*, pp. 306-311, 2003.

[6] R. C. Gonzalez, and R. E. Woods, *Digital Image Processing*, 2nd ed. NJ: Prentice Hall, 2002, pp. 85-86, 91-94, 550-554.

[7] N. Otsu, "A threshold selection method from gray level histogram," *IEEE Trans., SMC-9*, pp. 62-69, 1979.

[8] T. H. Kim, Y. S. Moon, and C. S. Han, "An efficient method of estimating edge locations with subpixel accuracy in noisy images," in *IEEE Region 10 Conference, TENCON*, pp. 589-592, 1999.